



**HAL**  
open science

## Plume-induced break-up of a subducting plate: Microcontinent formation without cessation of the subduction process

Alexander Koptev, Anouk Beniest, Taras Gerya, T.A. Ehlers, Laurent Jolivet,  
Sylvie Leroy

### ► To cite this version:

Alexander Koptev, Anouk Beniest, Taras Gerya, T.A. Ehlers, Laurent Jolivet, et al.. Plume-induced break-up of a subducting plate: Microcontinent formation without cessation of the subduction process. *Geophysical Research Letters*, 2019, 10.1029/2018GL081295 . hal-02325347v1

**HAL Id: hal-02325347**

**<https://hal.science/hal-02325347v1>**

Submitted on 25 Nov 2020 (v1), last revised 19 May 2021 (v2)

**HAL** is a multi-disciplinary open access archive for the deposit and dissemination of scientific research documents, whether they are published or not. The documents may come from teaching and research institutions in France or abroad, or from public or private research centers.

L'archive ouverte pluridisciplinaire **HAL**, est destinée au dépôt et à la diffusion de documents scientifiques de niveau recherche, publiés ou non, émanant des établissements d'enseignement et de recherche français ou étrangers, des laboratoires publics ou privés.

1 **Plume-induced break-up of a subducting plate:**  
2 **Microcontinent formation without cessation of the subduction process**  
3 **Alexander Koptev<sup>1,2</sup>, Anouk Beniést<sup>3</sup>, Taras Gerya<sup>4</sup>, Todd A. Ehlers<sup>1</sup>, Laurent Jolivet<sup>2</sup>, and**  
4 **Sylvie Leroy<sup>2</sup>**

5 <sup>1</sup> Department of Geosciences, University of Tübingen, Tübingen, Germany.

6 <sup>2</sup> Sorbonne Université, CNRS, Institut des Sciences de la Terre de Paris (ISTeP), Paris, France.

7 <sup>3</sup> Department of Earth Sciences, Vrije Universiteit Amsterdam, Amsterdam, The Netherlands.

8 <sup>4</sup> ETH-Zurich, Institute of Geophysics, Zurich, Switzerland.

9

10 Corresponding author: Alexander Koptev (alexander.koptev@ifg.uni-tuebingen.de)

11

12 **Key Points:**

- 13 • 3D thermo-mechanical modeling was performed to investigate the impact of the arrival of  
14 a mantle plume below a subducting lithospheric plate.
- 15 • The thermal and buoyancy effects of a mantle plume prove sufficient to induce the  
16 separation of a microcontinent from the subducting plate.
- 17 • The proposed scenario is consistent with a separation of the Apulian microcontinent from  
18 Africa during subduction of the Neo-Tethys.  
19

## 20 **Abstract**

21 Separation of microcontinents is explained by a ridge jump toward the passive margin as a  
22 possible consequence of plume-induced rheological weakening, ultimately leading to break-up  
23 followed by accretion of the oceanic crust along a new spreading center. In contrast to such a  
24 purely extensional case, the separation of continental micro-blocks from the main body of the  
25 African plate during its continuous northward motion and subduction under Eurasia is still  
26 poorly understood. Our numerical experiments show the thermal and buoyancy effects of mantle  
27 plume impingement on the bottom of the continental part of a subducting plate are sufficient to  
28 induce separation of an isolated micro-continental block from the main subducting continent,  
29 even during induced plate motion necessary for uninterrupted oceanic and continental  
30 subduction. Subsequent continental accretion occurs by decoupling upper-crustal nappes from  
31 the newly formed subducting microcontinent, which is in agreement with the Late Cretaceous –  
32 Eocene evolution of the eastern Mediterranean.

## 33 **Plain Language Summary**

34 Separation of micro-continental blocks from their parent continent is usually attributed to abrupt  
35 relocation of concentrated extension from the mid-oceanic ridge to the adjacent continental  
36 margin. In the context of extensional passive margin evolution, previous extensive numerical and  
37 analogue studies have revealed that hot upwelling mantle flow plays a key role in the mechanical  
38 weakening of the passive margin lithosphere needed to initiate a ridge jump. This, in turn, results  
39 in continental break-up and subsequent microcontinent isolation. However, the consequences of  
40 mantle plume impingement on the base of a moving lithospheric plate that is already involved  
41 into subduction are still unexplored quantitatively. Here we present the results of 3D thermo-  
42 mechanical models showing that even in the context of induced plate motion (contractional  
43 boundary conditions), which are necessary to sustain continuous convergence, thermal and  
44 buoyancy effects of the mantle plume emplaced at the bottom of the continental part of the  
45 subducting plate are sufficient to initiate continental break-up and the subsequent opening of a  
46 new oceanic basin that separates the micro-continental block from the main body of the  
47 continent. With these models, we show that it is physically possible to form microcontinents in a  
48 convergent setting without the cessation of subduction.

49

## 50 **1 Introduction**

51 Microcontinents are defined as independent blocks of continental lithosphere that are isolated  
52 from any other continental domains and are surrounded by ocean floor (Scrutton, 1976; Peron-  
53 Pinvidic & Manatschal, 2010). Jan Mayen in the Norwegian-Greenland Sea (Myhre et al., 1984;  
54 Gudlaugsson et al., 1988; Peron-Pinvidic et al., 2012; Blischke et al., 2016; Schiffer et al., 2018),  
55 the Seychelles in the Indian Ocean (Dickin et al., 1986; Plummer & Belle, 1995; Collier et al.,  
56 2009; Ganerød et al., 2011), and the East Tasman Plateau and the Gilbert Seamount Complex in  
57 the Tasman Sea (Exon et al., 1997; Gaina et al., 1998, 2003) are usually cited as “typical”  
58 examples of separated micro-continental blocks (Fig. 1a) as they are formed in a purely  
59 extensional tectonic setting. The best example of such microcontinents is the Jan Mayen platform  
60 separated from East Greenland in the Oligocene – Early Miocene due to a ridge jump toward the  
61 passive continental margin with the cessation of spreading at the existing mid-oceanic ridge  
62 (Lundin & Doré, 2002; Gaina et al., 2009). In this and certain other cases, rifting and

63 subsequent break-up along a passive margin is triggered by the thermal effect of an arriving  
64 mantle plume. The increase in temperature causes a decrease in the strength of the lithosphere  
65 that is large enough to re-localize the extension center from the mid-oceanic ridge toward the  
66 inner flank of the continental margin (Müller et al., 2001 and references therein). Apart from a  
67 severe weakening due to plume-induced reheating, intrinsic differences in lithospheric strength  
68 between different parts of the passive margin (Vink et al., 1984; Molnar et al., 2018) and plate  
69 reorganisation events (Whittaker et al., 2016) have also been considered to influence the  
70 segregation of continental fragments.

71 Another group of microcontinents refers to micro-blocks that are detached from the continental  
72 segment of lithosphere during continuous subduction of its oceanic counterpart under the active  
73 margin of the opposite continent (Fig. 1b). Natural examples have been found in the eastern  
74 Mediterranean, where an intricate assemblage of tectonic units implies that several continental  
75 fragments were successively separated from Africa and then accreted to the Eurasian margin  
76 (Sengör & Yilmaz, 1981; Dercourt et al., 1986; Barrier & Vrielynck, 2008; Menant et al., 2016;  
77 Barrier et al., 2018), while the Neo-Tethys was consumed by subduction (Takin, 1972; Dercourt  
78 et al., 1993; Hafkenscheid et al., 2006; Agard et al., 2011; Jolivet et al., 2016). In particular, the  
79 Apulian microcontinent detached from Africa in the Jurassic (Ricou, 1994; Frizon de Lamotte et  
80 al., 2011; Jolivet et al., 2016) and drifted away from Africa to subduct and collide with Eurasia  
81 in the Late Cretaceous – Eocene resulting in the building of the Taurides in the east and the  
82 Hellenides in the west (Dercourt et al., 1986; Jolivet et al., 2003; Van Hinsbergen et al., 2005).  
83 Later, in the Late Eocene – Early Oligocene, continental rifting started in the Red Sea and Gulf  
84 of Aden (Roger et al., 1989; Ghebreab, 1998; Watchorn et al., 1998; Leroy et al., 2012), which  
85 ultimately led to Africa-Arabia break-up in the Early Miocene (Joffe & Garfunkel, 1987;  
86 Bosworth et al., 2005; Leroy et al., 2010; Mohriak & Leroy, 2013). In contrast to the Apulian  
87 microcontinent, Arabia separated from Africa at the very last stage of the Neo-Tethys during  
88 Africa/Arabia-Eurasia collision (Jolivet & Faccenna, 2000; Bellahsen et al., 2003; Koptev et al.,  
89 2018c). The northern Appalachians (e.g. Van Staal et al. 2009, 2012) and southern Alaska (e.g.  
90 Plafker & Berg, 1994; Bruhn et al., 2004; Enkelmann et al., 2017) are other classical examples of  
91 complex mountain belts formed by accretion of tectonic terranes during the Early to Middle  
92 Paleozoic and in the Cretaceous – Cenozoic, respectively.

93 Over the last decade, several numerical studies have been performed to investigate the origin of  
94 microcontinents in extensional settings. Possible mechanisms for intra-oceanic ridge-jumps  
95 (Mittelstaedt et al., 2008, 2011; d'Acremont et al., 2010) and for mid-oceanic ridge jumps to the  
96 passive continental margins have been explored by both numerical (Beniest et al., 2017a, 2017b;  
97 Lavecchia et al., 2017) and analogue (Dubinin et al., 2018) modeling studies. However, it is still  
98 not apparent how microcontinents form in a convergent tectonic system like Africa during its  
99 motion toward Eurasia. Part of the enigmatic nature of these microcontinents is the overall  
100 contractional tectonic regime in which diverging forces act locally to separate slivers of  
101 continental lithosphere from the main body. Such extensional episodes resulting in the stripping  
102 of the microcontinents have been attributed to the push of mantle plumes periodically arriving at  
103 the base of the African lithosphere (Faccenna et al., 2013; Jolivet et al., 2016). These mantle  
104 plume events and associated large igneous provinces (LIPs) of the past 180-300 Myr (Torsvik et  
105 al., 2006; Burke et al., 2008; Jourdan et al., 2008; Ernst, 2014) are related to a long-lived thermal  
106 upwelling through the mantle beneath Africa (Forte & Mitrovica, 2001) that is often referred as  
107 “African Superplume” (Gurnis et al., 2000). It likely emanates from a large-scale, low seismic  
108 velocity province at the core-mantle boundary (Ritsema et al., 1999). The recent numerical

109 models show that the mantle superplumes might be a result of an upwelling return flow in  
110 response to deeply subducting slabs penetrating the lower mantle (Zhang et al., 2010; Heron et  
111 al., 2015; Dal Zilio, 2018; Dal Zilio et al., 2018).

112 However, the exact consequences of the arrival of the ascending mantle plume at the base of the  
113 continental part of the subducting lithospheric plate on microcontinents separation and their  
114 subsequent subduction and/or accretion at the opposite continental margin have never been  
115 estimated quantitatively and thus remain in many aspects unclear.

116 Here we present the results of a 3D high-resolution thermo-mechanical model that investigates  
117 the effect of mantle plume impingement on the base of an already moving subducting continental  
118 lithospheric plate that contains an oceanic domain continuously sinking below the opposite  
119 continent. With these experiments we test the hypothesis that the buoyancy and thermal  
120 influence of a mantle plume are sufficient to induce separation and isolation of micro-continental  
121 blocks even in the context of uninterrupted plates' convergence.

122

## 123 **2 Numerical model description**

124 We produced the simulations presented in this contribution using the viscous-plastic code  
125 "I3ELVIS" (see Supporting information, and Gerya & Yuen (2007) and Gerya (2010) for more  
126 details).

127 The model domain (Fig. 2) measures  $1000 \times 400 \times 200$  km in the x, y and z dimensions. This  
128 model box is resolved by  $501 \times 201 \times 101$  grid points thus offering a spatial resolution of ca. 2 km  
129 per grid cell in each direction.

130 The initial model setup consists of two parts: 1) an overriding continental lithosphere (400 km  
131 wide), and 2) a subducting slab that includes both oceanic and continental lithospheric segments  
132 (200 km and 400 km wide). The continental crust consists of 20 km of felsic (wet quartzite  
133 ductile flow law) upper crust and 15 km of mafic (plagioclase flow law) lower crust. The oceanic  
134 crust is represented by 8 km of basalt and gabbroic rocks (plagioclase flow law). Both the  
135 lithospheric and the sublithospheric mantle are composed of anhydrous peridotite (dry olivine  
136 flow law).

137 The velocity boundary conditions are free slip at both the front and back sides of the model box  
138 ( $y=0$  km and  $y=400$  km). The right boundary ( $x=1000$  km) uses a uniform and constant-in-time  
139 x-parallel velocity (varied from 0 to 4.5 cm/yr), which defines the material influx. The left  
140 boundary ( $x=0$  km) is fixed, meaning zero displacement in all directions. Mass conservation is  
141 ensured by the material outflux through the upper and lower permeable boundaries ( $z=0$  and  
142  $z=200$  km).

143 The laterally uniform thermal structure of the continents is piece-wise linear with  $0^\circ\text{C}$  at the  
144 surface (i.e. at the boundary between sticky air and upper crust) and  $1350^\circ\text{C}$  at 100 km ("normal"  
145 continental geotherm) or 90 km depth ("elevated" continental geotherm). The initial thermal  
146 distribution in the oceanic lithosphere is defined by a half-space cooling age at 60 Ma (Turcotte  
147 & Schubert, 2002). Both continental and oceanic lithospheres overlay a sublithospheric mantle  
148 with an initial adiabatic temperature gradient of  $\sim 0.5^\circ\text{C}/\text{km}$ .

149 We start our modeling procedure with the "no-plume" model **1** (see Table S1), including a  
150 "normal" continental geotherm ( $1350^\circ\text{C}$  isotherm at 100 km depth) in both the overriding and

151 subducting plates and a horizontal material influx at the right model side ( $V_x$ ) of 4.5 cm/yr. Next,  
152 we introduce in this setup a mantle plume anomaly below the subducting continent. This  
153 anomaly is characterized by different initial temperatures – “normal” (1900°C, model 2) and  
154 relatively “high” (2000°C, model 3). Finally, we test the impact of an “elevated” continental  
155 geotherm (1350°C isotherm at 90 km) with the experiments characterized by a “normal”  
156 (1900°C) plume temperature and different boundary velocities of material influx ( $V_x$ ) varying  
157 from 4.5 cm/yr (model 4) through 3.0 cm/yr (model 5), 1.5 cm/yr (model 6) and 0.3 cm/yr  
158 (model 7) to 0 cm/yr (model 8). Note that in these experiments (model 4-8), the “elevated”  
159 continental geotherm is only applied to the subducting plate while the continental lithosphere of  
160 the overriding plate keeps the “normal” thermal gradient.

161

### 162 **3 Results**

163 In the “no plume” experiment (model 1, Fig. 3a), subduction of the oceanic lithosphere is  
164 followed by sinking of the continental part of the subducting plate. Initiation of the continental  
165 subduction coincides in time (~5 Myr) with the onset of partial melting of the hydrated mantle  
166 material composing the initial “weak zone” seeded between the overriding and subducting plates.  
167 At a later stage of the system’s development (~10 Myr), the subducted continent reaches depths  
168 of 100 km where its upper crust is also involved in melting. Similar temporal transitions of  
169 subduction-related magmatism from mafic with mantle origin to felsic with crustal origin  
170 geochemical signature are reported in the Malayer-Boroujerd plutonic complex in western Iran  
171 (Deevsalar et al., 2018).

172 In the remaining experiments (models 2-8; Figs. 3b-d, 4-5), the mantle plume seeded by a  
173 temperature anomaly at the bottom of the model box ascends quickly (~0.1 My) to the base of the  
174 continental part of the overlying plate. The thermal impact of the upwelling hot mantle leads to  
175 partial melting of not only the plume itself but also of adjacent lithospheric and sublithospheric  
176 material. For the models with the “normal” temperature gradient (models 2-3), this mixed melt is  
177 attached to the bottom of the lithosphere and moves together with the plate into the subduction  
178 zone (Fig. 3b-c) without a strong influence on the system’s evolution compared to that of the “no  
179 plume” model 1 (Fig. 3a). Note, however, that model 3 with a relatively “hot” thermal anomaly  
180 (initial temperature of 2000°C) shows a deeper penetration of the plume into the lithospheric  
181 mantle and a more intense percolation of melts that are continuously generated from the melt-  
182 bearing material, thereby resulting in the underplating of mafic magmas at the crust-mantle  
183 boundary (Fig. 3c).

184 An increase of the continental geotherm leads to large changes in the system’s behavior (models  
185 4-8 with “elevated” thermal gradient; Figs. 3d, 4-5, S1-2). Mantle plume impingement on the  
186 bottom of the lithosphere (Fig. S1a) is followed by fast (~25 cm/yr) penetration of hot plume  
187 material through the mantle (Fig. S1b). This leads to thinning of the continental lithosphere and  
188 decompressional melting of both lithospheric and asthenospheric mantle in the area of plume  
189 emplacement and along the spontaneously localizing trench-parallel rifting zone that crosses the  
190 entire model domain (Fig. 4a; Fig. S2b). This spontaneous rifting characterized by a quick  
191 transition in time from wide to narrow mode (Fig. S2a-b) likely results from the presence of  
192 intraplate extensional stresses produced by both the plume-induced divergence and the growing  
193 pulling force of the continuously subducting oceanic slab. These extensional stresses result in a  
194 rapid and focused continental break-up in less than 0.5 Myr after the model’s onset (Fig. 4b).

195 Note that the break-up first occurs in the central part of the model domain (i.e. above the plume  
196 apex) while in the peripheral segments the transition from the pre-break-up rifting to post-break  
197 spreading is delayed by ~0.2-0.3 Myr (Figs. S1c, S2c). This break-up leads to the separation of  
198 the newly formed microcontinent from the main continental body of the subducting plate (Fig.  
199 4c).

200 The combined effect of the plume push and pulling force of a negatively buoyant slab results in a  
201 lateral displacement of the separated micro-block that is considerably faster (~10-15 cm/yr) than  
202 the imposed boundary condition velocity (~4.5 cm/yr) at the right side of the subducting plate  
203 (Fig. S3). Therefore, despite this continuous external push, a trench-parallel oceanic basin opens  
204 within a few Myr (Figs. S2d) reaching a width of ~100 kilometers wide above the plume  
205 impingement point (Fig. S1d).

206 The sensitivity analysis of the previous results with different boundary conditions (models **5-8**)  
207 shows that fast plume-induced continental break-up occurs within 0.5 Myr in all experiments,  
208 regardless the magnitude of the applied external push (Fig. 5). In contrast, the maximum width of  
209 the newly formed ocean basin varies as a function of the boundary velocities: it increases from  
210 100 km to 200 km as the external push decreases from 3.0 cm/yr to 0 cm/yr (Fig. 5).

211 As soon as the initial ocean is completely subducted, the separated micro-continental block starts  
212 to sink below the overriding continental plate (Fig. 4d). After having reached its maximum depth  
213 (~100 km), buoyant upper crust of subducting microcontinent decouples from the lower crust  
214 and mantle and migrates upwards to the surface in a return flow along the subduction channel  
215 (Fig. 4e-f). The fluid-saturated oceanic crust of the newly formed basin, which is also involved in  
216 the subduction, may play a lubricating role in this exhumation process. Note that more advanced  
217 exhumation occurs in the central segment of the model domain (Fig. 4f) possibly due to the  
218 thermal impact of the mantle plume. A comparison of the model sensitivity to different boundary  
219 velocities of material influx (models **4-7**) shows that faster subduction leads to an earlier onset of  
220 exhumation of the upper micro-continental crust. The time of exhumation initiation varies from  
221 7-9 Myr through 12 Myr to 45 Myr with a decrease of applied push ( $V_x$ ) from 4.5-3.0 cm/yr  
222 through 1.5 cm/yr to 0.3 cm/yr (see Figs. 3d, 4e, 5a-c). Note also that in the case of relatively  
223 “fast” subduction (models **4-5**;  $V_x=4.5-3.0$  cm/yr), exhumation of the micro-continental upper  
224 crust occurs simultaneously with the subduction of the main continent. As a result, exhumed  
225 micro-continental crust overthrusts the crust of the subducted main continent while newly  
226 formed oceanic crust is deeply (>100 km) subducted (Figs. 3d, 4f, 5a). This is different for the  
227 “intermediate” case (model **6**,  $V_x=1.5$  cm/yr) where the exhumed crust of the microcontinent is  
228 underlain by oceanic material of the new basin because the exhumation process was already  
229 ongoing before subduction of the main continental body (Fig. 5b). In the “slow” subduction case  
230 of model **7** ( $V_x=0.3$  cm/yr), micro-continental upper crust accretes at the boundary between the  
231 subducting and upper plates without deep subduction below the overriding continent (Fig. 5c).

232 Even in the absence of external material influx (model **8**;  $V_x=0$  cm/yr) an oceanic subduction is  
233 quickly initiated because of the gravitational slab-pull force. However, the active subduction  
234 continues only until the microcontinent reaches the overriding plate (3 Myr after onset of the  
235 experiment). After 10 Myr, the subduction process is stopped and the system can be considered  
236 as steady-state (Fig. 5d). This implies that an external push and contractional boundary  
237 conditions are necessary to sustain ongoing subduction of the oceanic lithosphere and isolated  
238 micro-block(s) as well as their moving towards the opposite continent, as is the case for the  
239 Africa-Eurasia convergence.

240

241 **4 Discussion**

242 The formation of isolated micro-continental blocks and their subsequent accretion are common  
243 in the geologic record. The separation of microcontinents in a purely extensional setting of the  
244 passive rifted margins is attributed to a ridge jump toward the continent due to rheological  
245 weakening of the passive margin lithosphere resulting from the thermal impact of the mantle  
246 plume (Fig. 1a). Repeated jumps of mid-oceanic ridges toward nearby hot spots within oceanic  
247 lithosphere have been reproduced numerically by Mittelstaedt et al. (2008, 2011) and observed  
248 by d'Acremont et al. (2010). In the context of the continental lithosphere, the 2D thermo-  
249 mechanical modeling by Lavecchia et al. (2017) showed an abandonment of the rift initially  
250 localized in a pre-existing zone of lithospheric weakness and associated rift jump toward the  
251 thermally activated mantle plume. Mantle upwelling, thus, was confirmed to be one of the key  
252 factors in the contrasting continental rifting characterized by both “passive/amagmatic” and  
253 “active/magmatic” branches (see also 3D experiments by Koptev et al., 2015, 2016, 2018a,  
254 2018b) that may further evolve into break-up centers embracing isolated continental block  
255 (Beniest et al., 2017b). In analogue models, a complete separation of the micro-continental body  
256 from a parent continent is also strongly connected to the thermal weakening due to the presence  
257 of a hot spot (Dubinin et al., 2018).

258 Continental micro-blocks separated from the main body of the African plate during its northward  
259 motion toward Eurasia accommodated by uninterrupted oceanic and continental subduction  
260 define a second type of microcontinent behavior (Fig. 2b). The northern margin of Africa is  
261 known to have experienced fragmentation since the Paleozoic when a series of small continental  
262 plates have been rifted away from Gondwana (the Avalonia and Armorica terranes in the  
263 Ordovician, the European Hunic terranes in the Silurian, and the Cimmerian blocks in the  
264 Permian) and subsequently accreted along the active southern margin of Laurussia (Matte, 2001;  
265 Stampfli & Borel, 2002; Von Raumer et al., 2003). The European Hunic terranes have been  
266 detached from the active northern Gondwana margin by oceanward migration of the arc-trench  
267 systems due to slab rollback of the Rheic ocean (Stampfli & Borel, 2002; Stampfli et al., 2002)  
268 and thus were bounded by different – active and passive – plate margins. Evolution and possible  
269 mechanisms for formation of such back-arc basins separating the volcanic arcs from the  
270 mainland have been thoroughly investigated by several numerical studies over the last decade  
271 (Clark et al., 2008; Sizova et al., 2010; Gerya & Meilick, 2011; Dal Zilio et al., 2018). In  
272 contrast, other continental domains separated from northern Gondwana in the Paleozoic (the  
273 Avalonia and Armorica terranes, and the Cimmerian blocks) had initially two passive margins  
274 (Matte, 2001; Stampfli & Borel, 2002) similar to the Mesozoic Apulian microcontinent  
275 segregated from the passive African margin (Jolivet et al., 2016). Formation of these  
276 microcontinents with two passive margins but formed on the subducting plate (Fig. 1b) is not  
277 apparent since they represent the results of extensional processes while developed in an overall  
278 context of convergence.

279 In the 3D thermo-mechanical numerical results presented here, we combine a pre-imposed  
280 convergence rate with the self-driven dynamics of a mantle plume. The push of the mantle plume  
281 impinged at the base of the African plate triggering local extension is shown to be sufficient for  
282 micro-block separation. Our results reveal the key role of the initial thermal structure of the  
283 overlying continent in this process because continental break-up and microcontinent separation



284 occurs only under condition of a relatively “elevated” geotherm (see models **4-8**; Figs. 3d, 4-5).  
285 In contrast, variations in plume temperature do not appear to be crucial (models **2-3**; Fig. 3b-c).  
286 The presence of a continuous external push (possibly resulting from a large-scale mantle flow  
287 due to the large plume postulated by Jolivet et al. (2016)) is shown to be indispensable to sustain  
288 continental subduction of the separated micro-block (compare Fig. 5a-c and Fig. 5d). In the final  
289 stages of the experiments, the subduction of the separated micro-block is followed by tectonic  
290 exhumation of the upper crust (Fig. 5a-c). This is consistent with continental accretion in the  
291 eastern Mediterranean zone during the Cenozoic where it has occurred by decoupling crustal  
292 nappes from the subducting continental lithosphere in contrast to the eastern Anatolia  
293 characterized by “true” collisional events (Menant et al., 2018).

294 The thermo-mechanical models presented here consider the mantle plume as a necessary  
295 ingredient for the generation of locally-extensional tectonics in a regionally-compressive  
296 environment that ultimately results in microcontinent formation. Note though, that we do not rule  
297 out other factors possibly contributing to the separation of a micro-block from the subducting  
298 plate such as (1) regional-scale plate reorganization associated to sharp convergence acceleration  
299 (Agard et al., 2006, 2007) or (2) lateral transition from subduction to collision along the  
300 convergent boundary (Decourt et al., 1993; Bellahsen et al., 2003; Koptev et al., 2018c) in the  
301 presence of (3) pre-existing zones of weakness (Dixon et al., 1987; Ligi et al., 2012).

302

## 303 **5 Conclusions**

304 The modeling results presented here reveal that even in a convergent tectonic setting, an  
305 upwelling flow of hot mantle material can trigger localized extension, rifting and breakup. This  
306 ultimately leads to the opening of a new oceanic basin that separates a micro-continental sliver  
307 from the main continent belonging to a subducting lithospheric plate. The scenario evaluated  
308 involves plume-induced separation of a microcontinent away from the main continent during  
309 uninterrupted subduction. This can be compared to the Paleozoic – Cenozoic evolution of Africa,  
310 which is characterized by subsequent separation of several micro-continental pieces while  
311 subduction of the oceanic and continental lithosphere below the Eurasian margin was ongoing.

312

## 313 **Acknowledgments**

314 We thank two reviewers for their helpful and constructive comments. This study is co-funded by  
315 the Advanced ERC Grant 290864 RHEOLITH (L. Jolivet – A. Koptev) and ERC Consolidator  
316 Grant 615703 EXTREME (T. Ehlers – A. Koptev). The numerical simulations were performed  
317 on the ERC-funded SGI Ulysse cluster of ISTeP. The computer code I3ELVIS used to generate  
318 our 3D thermo-mechanical numerical model is provided in Gerya (2010). Open source software  
319 ParaView (<http://www.paraview.org>) was used for 3D visualization. The figures in the  
320 supporting information contain the numerical simulation data.

321

322 **References**

- 323 Agard, P., Jolivet, L., Vrielynck, B., Burov, E., & Monie, P. (2007). Plate acceleration: the  
 324 obduction trigger? *Earth and Planetary Science Letters*, 258(3–4), 428–441.  
 325 doi:10.1016/j.epsl.2007.04.002
- 326 Agard, P., Monié, P., Gerber, W., Omrani, J., Molinaro, M., Meyer, B., et al. (2006). Transient,  
 327 synobduction exhumation of Zagros blueschists inferred from P-T, deformation, time, and  
 328 kinematic constraints: Implications for Neotethyan wedge dynamics. *Journal of Geophysical*  
 329 *Research: Solid Earth*, 111, B11. doi:10.1029/2005JB004103
- 330 Agard, P., Omrani, J., Jolivet, L., Whitechurch, H., Vrielynck, B., Spakman, W., et al. (2011).  
 331 Zagros orogeny: a subduction-dominated process. *Geological Magazine*, 148(5–6), 692–725.  
 332 doi:10.1017/S001675681100046X
- 333 Barrier, E., & Vrielynck, B. (2008). Paleotectonic maps of the Middle East. *Atlas of 14 Maps,*  
 334 *Middle East Basin Evolution Programme*. Paris.
- 335 Barrier, E., Vrielynck, B., Brouillet, J. F., & Brunet, M. F. (2018). Paleotectonic reconstruction  
 336 of the Central Tethyan Realm. Tectono-sedimentary-palinspastic maps from Late Permian to  
 337 Pliocene. *Atlas of 20 maps (scale: 1/15 000 000), CCGM/CGMW*. <http://www.ccgm.org>.
- 338 Bellahsen, N., Faccenna, C., Funicello, F., Daniel, J. M., & Jolivet, L. (2003). Why did Arabia  
 339 separate from Africa? Insights from 3-D laboratory experiments. *Earth Planetary Science*  
 340 *Letters*, 216(3), 365–381. doi:10.1016/S0012-821X(03)00516-8
- 341 Beniést, A., Koptev, A., & Burov, E. (2017a). Numerical models for continental break-up:  
 342 Implications for the South Atlantic. *Earth and Planetary Science Letters*, 461, 176–189.  
 343 doi:10.1016/j.epsl.2016.12.034
- 344 Beniést, A., Koptev, A., Leroy, S., Sassi, W., & Guichet, X. (2017b). Two-branch break-up  
 345 systems by a single mantle plume: Insights from numerical modeling. *Geophysical Research*  
 346 *Letters*, 44(19), 9589–9597. doi:10.1002/2017GL074866
- 347 Blischke, A., Gaina, C., Hopper, J. R., Péron-Pinvidic, G., Brandsdottir, B., Guarnieri, P., et al.  
 348 (2016). The Jan Mayen microcontinent: an update of its architecture, structural development and  
 349 role during the transition from the Ægir Ridge to the mid-oceanic Kolbeinsey Ridge. *Geological*  
 350 *Society London, Special Publications*, 447, SP447–5. doi:10.1144/SP447.5
- 351 Bosworth, W., Huchon, P., & McClay, K. (2005). The Red Sea and Gulf of Aden basins. *Journal*  
 352 *of African Earth Sciences*, 43(1–3), 334–378. doi:10.1016/j.jafrearsci.2005.07.020
- 353 Bruhn, R. L., Pavlis, T. L., Plafker, G., & Serpa, L. (2004). Deformation during terrane accretion  
 354 in the Saint Elias orogen, Alaska. *Geological Society of America Bulletin*, 116(7–8), 771–787.  
 355 doi:10.1130/B25182.1
- 356 Burg, J. P., & Gerya, T. V. (2005). The role of viscous heating in Barrovian metamorphism of  
 357 collisional orogens: thermomechanical models and application to the Lepontine Dome in the  
 358 Central Alps. *Journal of Metamorphic Geology*, 23(2), 75–95. doi:10.1111/j.1525-  
 359 1314.2005.00563.x
- 360 Burke, K., Steinberger, B., Torsvik, T. H., & Smethurst, M. A. (2008). Plume generation zones  
 361 at the margins of large low shear velocity provinces on the core–mantle boundary. *Earth and*  
 362 *Planetary Science Letters*, 265(1–2), 49–60. doi:10.1016/j.epsl.2007.09.042

- 363 Clark, S. R., Stegman, D., & Dietmar, R. M. (2008). Episodicity in back-arc tectonic regimes.  
 364 *Physics of the Earth and Planetary Interiors*, 171(1–4), 265–279.  
 365 doi:10.1016/j.pepi.2008.04.012
- 366 Collier, J. S., Minshull, T. A., Hammond, J. O. S., Whitmarsh, R. B., Kendall, J., Sansom, V., et  
 367 al. (2009). Factors influencing magmatism during continental breakup: New insights from a  
 368 wide-angle seismic experiment across the conjugate Seychelles-Indian margins. *Journal of*  
 369 *Geophysical Research: Solid Earth*, 114, B3. doi:10.1029/2008JB005898
- 370 Connolly, J. A. (2005). Computation of phase equilibria by linear programming: a tool for  
 371 geodynamic modeling and its application to subduction zone decarbonation. *Earth and Planetary*  
 372 *Science Letters*, 236(1–2), 524–541. doi:10.1016/j.epsl.2005.04.033
- 373 Crameri, F., Schmeling, H., Golabek, G. J., Duretz, T., Orendt, R., Buitter, S. J. H., et al. (2012).  
 374 A comparison of numerical surface topography calculations in geodynamic modelling: an  
 375 evolution of the “sticky air” method. *Geophysical Journal International*, 189(1), 38–54.  
 376 doi:10.1111/j.1365-246X.2012.05388.x
- 377 d'Acromont, E., Leroy, S., Maia, M., Gente, P., & Autin, J. (2010). Volcanism, jump and  
 378 propagation on the Sheba ridge, eastern Gulf of Aden: segmentation evolution and implications  
 379 for oceanic accretion processes. *Geophysical Journal International*, 180(2), 535–551.  
 380 doi:10.1111/j.1365-246X.2009.04448.x
- 381 Dal Zilio, L. (2018). Subduction-driven Earth machine. *Nature Geoscience*, 11(4), 229.  
 382 doi:10.1038/s41561-018-0102-z
- 383 Dal Zilio, L., Faccenda, M., & Capitanio, F. (2018). The role of deep subduction in  
 384 supercontinent breakup. *Tectonophysics*, 746, 312–324. doi:10.1016/j.tecto.2017.03.006
- 385 Deevsalar, R., Shinjo, R., Liégeois, J. P., Valizadeh, M. V., Ahmadian, J., Yeganehfar, H., et al.  
 386 (2018). Subduction-related mafic to felsic magmatism in the Malayer-Boroujerd plutonic  
 387 complex, western Iran. *Swiss Journal of Geosciences*, 111, 269–293. doi:10.1007/s00015-017-  
 388 0287-y
- 389 Dercourt, J., Ricou, L. E., & Vrielynck, B. (1993). Atlas Tethys Palaeoenvironmental Maps.  
 390 *BEICIP-FRANLAB Gauthier-Vollars*, Paris.
- 391 Dercourt, J., Zonenshain, L. P., Ricou, L.-E., Kazmin, V. G., Le Pichon, X., Knipper, A. L., et al.  
 392 (1986). Geological evolution of the Tethys belt from the Atlantic to the Pamirs since the Lias.  
 393 *Tectonophysics*, 123(1–4), 241–315. doi:10.1016/0040-1951(86)90199-X
- 394 Dickin, A. P., Fallick, A. E., Halliday, A. N., Macintyre, R. M., & Stephens, W. E. (1986). An  
 395 isotopic and geochronological investigation of the younger igneous rocks of the Seychelles  
 396 microcontinent. *Earth and Planetary Science Letters*, 81(1), 46–56. doi:10.1016/0012-  
 397 821X(86)90099-3
- 398 Dixon, T. H., Stern, R. J., & Hussein, I. M. (1987). Control of Red Sea rift geometry by  
 399 Precambrian structures. *Tectonics*, 6(5), 551–571. doi.org/10.1029/TC006i005p00551
- 400 Dubinin, E. P., Grokholsky, A. L., & Makushkina, A. I. (2018). Physical modeling of the  
 401 formation conditions of microcontinents and continental marginal plateaus. *Izvestiya, Physics of*  
 402 *the Solid Earth*, 54(1), 66–78. doi:10.1134/S1069351318010056

- 403 Duretz, T., May, D. A., Gerya, T. V., & Tackley, P. J. (2011). Discretization errors and free  
 404 surface stabilization in the finite difference and marker-in-cell method for applied geodynamics:  
 405 A numerical study. *Geochemistry, Geophysics, Geosystems*, 12(7), Q07004.  
 406 doi:10.1029/2011GC003567
- 407 Enkelmann, E., Piestrzeniewicz, A., Falkowski, S., Stübner, K., & Ehlers, T. A. (2017).  
 408 Thermochemistry in southeast Alaska and southwest Yukon: Implications for North American  
 409 Plate response to terrane accretion. *Earth and Planetary Science Letters*, 457, 348–358.  
 410 doi:10.1016/j.epsl.2016.10.032
- 411 Ernst, R. E. (2014). *Large Igneous Provinces* (pp. 653). Cambridge, UK: Cambridge University  
 412 Press.
- 413 Exon, N. F., Berry, R. F., Crawford, A. J., & Hill, P. J. (1997). Geological evolution of the East  
 414 Tasman Plateau, a continental fragment southeast of Tasmania. *Australian Journal of Earth  
 415 Sciences*, 44(5), 597–608. doi:10.1080/08120099708728339
- 416 Faccenna, C., Becker, T. W., Jolivet, L., & Keskin, M. (2013). Mantle convection in the Middle  
 417 East: Reconciling Afar upwelling, Arabia indentation and Aegean trench rollback. *Earth and  
 418 Planetary Science Letters*, 375, 254–269. doi:10.1016/j.epsl.2013.05.043
- 419 Forte, A. M., & Mitrovica, J. X. (2001). Deep-mantle high-viscosity flow and thermochemical  
 420 structure inferred from seismic and geodynamic data. *Nature*, 410(6832), 1049–1056.  
 421 doi:10.1038/35074000
- 422 Frizon de Lamotte, D., Raulin, C., Mouchot, N., Christophe, J., Daveau, W., Blanpied, C., &  
 423 Ringenbach, J. C. (2011). The southernmost margin of the Tethys realm during the Mesozoic and  
 424 Cenozoic: Initial geometry and timing of the inversion processes. *Tectonics*, 30(3).  
 425 doi:10.1029/2010TC002691
- 426 Gaina, C., Gernigon, L., & Ball, P. (2009). Palaeocene-Recent plate boundaries in the NE  
 427 Atlantic and the formation of the Jan Mayen microcontinent. *Journal of the Geological Society*,  
 428 166(4), 601–616. doi:10.1144/0016-76492008-112
- 429 Gaina, C., Müller, R. D., Brown, B., & Ishihara, T. (2003). Microcontinent formation around  
 430 Australia. *Geological Society of America Special Paper*, 372, 405–416. doi:10.1111/j.1365-  
 431 246X.2007.03450.x
- 432 Gaina, C., Roest, W. R., Müller, R. D., & Symonds, P. (1998). The opening of the Tasman Sea: a  
 433 gravity anomaly animation. *Earth Interactions*, 2(4), 1–23. doi:10.1175/1087-  
 434 3562(1998)002<0001:TOOTTS>2.3.CO;2
- 435 Ganerød, M., Torsvik, T. H., Van Hinsbergen, D. J. J., Gaina, C., Cordu, F., Werner, S., et al.  
 436 (2011). Palaeoposition of the Seychelles microcontinent in relation to the Deccan Traps and the  
 437 Plume Generation Zone in Late Cretaceous-Early Palaeogene time. *Geological Society London,  
 438 Special Publication*, 357(1), 229–252. doi:10.1144/SP357.12
- 439 Gerya, T. V. (2013). Initiation of transform faults at rifted continental margins: 3D petrological-  
 440 thermomechanical modeling and comparison to the Woodlark Basin. *Petrology*, 21(6), 550–560.  
 441 doi:10.1134/S0869591113060039
- 442 Gerya, T. V. (2010). *Introduction to numerical geodynamic modelling* (pp. 345). Cambridge,  
 443 UK: Cambridge University Press.

- 444 Gerya, T. V, & Meilick, F. I. (2011). Geodynamic regimes of subduction under an active margin:  
445 effects of rheological weakening by fluids and melts. *Journal of Metamorphic Geology*, 29(1),  
446 7–31. doi:10.1111/j.1525-1314.2010.00904.x
- 447 Gerya, T. V, & Yuen, D. A. (2007). Robust characteristics method for modelling multiphase  
448 visco-elasto-plastic thermo-mechanical problems. *Physics of the Earth and Planetary Interiors*,  
449 163(1–4), 83–105. doi:10.1016/j.pepi.2007.04.015
- 450 Ghebreab, W. (1998). Tectonics of the Red Sea region reassessed. *Earth-Science Reviews*, 45(1–  
451 2), 1–44. doi:10.1016/S0012-8252(98)00036-1
- 452 Gudlaugsson, S. T., Gunnarsson, K., Sand, M., & Skogseid, J. (1988). Tectonic and volcanic  
453 events at the Jan Mayen Ridge microcontinent. *Geological Society London, Special Publication*,  
454 39(1), 85–93. doi:10.1144/GSL.SP.1988.039.01.09
- 455 Gurnis, M., Mitrovica, J. X., Ritsema, J., & van Heijst, H. J. (2000). Constraining mantle density  
456 structure using geological evidence of surface uplift rates: The case of the African superplume.  
457 *Geochemistry, Geophysics, Geosystems*, 1(7), 1020. doi:10.1029/1999GC000035
- 458 Hafkenscheid, E., Wortel, M. J. R., & Spakman, W. (2006). Subduction history of the Tethyan  
459 region derived from seismic tomography and tectonic reconstructions. *Journal of Geophysical*  
460 *Research: Solid Earth*, 111, B8. doi:10.1029/2005JB003791
- 461 Heron, P. J., Lowman, J. P., & Stein, C. (2015). Influences on the positioning of mantle plumes  
462 following supercontinent formation. *Journal of Geophysical Research: Solid Earth*, 120(5),  
463 3628–3648. doi:10.1002/2014JB011727
- 464 Joffe, S. A. M., & Garfunkel, Z. V. I. (1987). Plate kinematics of the circum Red Sea - a re-  
465 evaluation. *Tectonophysics*, 141(1–2), 5–22. doi:10.1016/0040-1951(87)90171-5
- 466 Jolivet, L., & Faccenna, C. (2000). Mediterranean extension and the Africa-Eurasia collision.  
467 *Tectonics*, 19(6), 1095–1106. doi:10.1029/2000TC900018
- 468 Jolivet, L., Faccenna, C., Agard, P., Frizon De Lamotte, D., Menant, A., Sternai, P., &  
469 Guillocheau, F. (2016). Neo-Tethys geodynamics and mantle convection: from extension to  
470 compression in Africa and a conceptual model for obduction. *Canadian Journal of Earth*  
471 *Sciences*, 53(11), 1–15. doi:10.1139/cjes-2015-0118
- 472 Jolivet, L., Faccenna, C., Goffe, B., Burov, E., & Agard, P. (2003). Subduction tectonics and  
473 exhumation of high-pressure metamorphic rocks in the Mediterranean orogens. *American*  
474 *Journal of Science*, 303(5), 353–409. doi:10.2475/ajs.303.5.353
- 475 Jourdan, F., Féraud, G., Bertrand, H., Watkeys, M. K., & Renne, A. P. (2008). The 40Ar/39Ar  
476 ages of the sill complex of the Karoo large igneous province: Implications for the Pliensbachian-  
477 Toarcian climate change. *Geochemistry, Geophysics, Geosystems*, 9(6), Q06009.  
478 doi:10.1029/2008GC001994
- 479 Katz, R. F., Spiegelman, M., & Langmuir, C. H. (2003). A new parameterization of hydrous  
480 mantle melting. *Geochemistry, Geophysics, Geosystems*, 4(9), 1073.  
481 doi:10.1029/2002GC000433
- 482 Koptev, A., Burov, E., Calais, E., Leroy, S., Gerya, T., Guillou-Frottier, L., & Cloetingh, S.  
483 (2016). Contrasted continental rifting via plume-craton interaction: Applications to Central East  
484 African Rift. *Geoscience Frontiers*, 7(2), 221–236. doi:10.1016/j.gsf.2015.11.002

- 485 Koptev, A., Burov, E., Gerya, T., Le Pourhiet, L., Leroy, S., Calais, E., & Jolivet, L. (2018a).  
 486 Plume-induced continental rifting and break-up in ultra-slow extension context: Insights from 3D  
 487 numerical modeling. *Tectonophysics*, 746, 121–137. doi:10.1016/j.tecto.2017.03.025
- 488 Koptev, A., Calais, E., Burov, E., Leroy, S., & Gerya, T. (2015). Dual continental rift systems  
 489 generated by plume-lithosphere interaction. *Nature Geoscience*, 8(5), 388–392.  
 490 doi:10.1038/NGEO2401
- 491 Koptev, A., Cloetingh, S., Gerya, T., Calais, E., & Leroy, S. (2018b). Non-uniform splitting of a  
 492 single mantle plume by double cratonic roots: Insight into the origin of the central and southern  
 493 East African Rift System. *Terra Nova*, 30(2), 125–134. doi:10.1111/ter.12317
- 494 Koptev A., Gerya, T., Calais, E., Leroy, S., & Burov, E. (2018c). Afar triple junction triggered  
 495 by plume-assisted bi-directional continental break-up. *Scientific Reports*, 8(1), 14742.  
 496 doi:10.1038/s41598-018-33117-3
- 497 Lavecchia, A., Thieulot, C., Beekman, F., Cloetingh, S., & Clark, S. (2017). Lithosphere erosion  
 498 and continental breakup: Interaction of extension, plume upwelling and melting. *Earth and*  
 499 *Planetary Science Letters*, 467, 89–98. doi:10.1016/j.epsl.2017.03.028
- 500 Leroy, S., d'Acremont, E., Tiberi, C., Basuyau, C., Autin, J., Lucazeau, F., & Sloan, H. (2010).  
 501 Recent off-axis volcanism in the eastern Gulf of Aden: implications for plume-ridge interaction.  
 502 *Earth Planetary Science Letters*, 293(1–2), 140–153. doi:10.1016/j.epsl.2010.02.036
- 503 Leroy, S., Razin, P., Autin, J., Bache, F., D'Acremont, E., Watremez, L., et al. (2012). From  
 504 rifting to oceanic spreading in the Gulf of Aden: a synthesis. *Arabian Journal of Geosciences*,  
 505 5(5), 859–901. doi:10.1007/s12517-011-0475-4
- 506 Ligi, M., Bonatti, E., Bortoluzzi, G., Cipriani, A., Cocchi, L., Caratori Tontini, F., et al. (2012).  
 507 Birth of an ocean in the Red Sea: Initial pangs. *Geochemistry, Geophysics, Geosystems*, 13(8),  
 508 Q08009. doi.org/10.1029/2012GC004155
- 509 Lundin, E., & Doré, A. G. (2002). Mid-Cenozoic post-breakup deformation in the 'passive'  
 510 margins bordering the Norwegian-Greenland Sea. *Marine and Petroleum Geology*, 19(1), 79–93.  
 511 doi:10.1016/S0264-8172(01)00046-0
- 512 Matte, P. (2001). The Variscan collage and orogeny ( $480 \pm 290$  Ma) and the tectonic definition  
 513 of the Armorica microplate: a review. *Terra Nova*, 13(2), 122–128. doi:10.1046/j.1365-  
 514 3121.2001.00327.x
- 515 Menant, A., Jolivet, L., & Vrielynck, B. (2016). Kinematic reconstructions and magmatic  
 516 evolution illuminating crustal and mantle dynamics of the eastern Mediterranean region since the  
 517 late Cretaceous. *Tectonophysics*, 675, 103–140. doi:10.1016/j.tecto.2016.03.007
- 518 Menant, A., Jolivet, L., Tuduri, J., Loiselet, C., Bertrand, G., & Guillou-Frottier, L. (2018). 3D  
 519 subduction dynamics: A first-order parameter of the transition from copper- to gold-rich deposits  
 520 in the eastern Mediterranean region. *Ore Geology Reviews*, 94, 118–135.  
 521 doi:10.1016/j.oregeorev.2018.01.023
- 522 Mittelstaedt, E., Ito, G., & Behn, M. D. (2008). Mid-ocean ridge jumps associated with hotspot  
 523 magmatism. *Earth and Planetary Science Letters*, 266(3–4), 256–270.  
 524 doi:10.1016/j.epsl.2007.10.055

- 525 Mittelstaedt, E., Ito, G., & van Hunen, J. (2011). Repeat ridge jumps associated with plume-ridge  
526 interaction, melt transport and ridge migration. *Journal of Geophysical Research: Solid Earth*,  
527 116, B1. doi:10.1029/2010JB007504
- 528 Mohriak, W. U., & Leroy, S. (2013). Architecture of rifted continental margins and break-up  
529 evolution: insights from the South Atlantic, North Atlantic and Red Sea-Gulf of Aden conjugate  
530 margins. *Geological Society London, Special Publications*, 369, SP369-17.  
531 doi:10.1144/SP369.17
- 532 Molnar, N. E., Cruden, A. R., & Betts, P. G. (2018). Unzipping continents and the birth of  
533 microcontinents. *Geology*, 46(5), 451–454. doi:10.1016/j.earscirev.2010.01.002.2
- 534 Müller, R. D., Gaina, C., Roest, W., & Hansen, D. L. (2001). A recipe for microcontinent  
535 formation. *Geology*, 29(3), 203–206. doi:10.1130/0091-  
536 7613(2001)029<0203:ARFMF>2.0.CO;2
- 537 Myhre, A. M., Eldholm, O., & Sundvor, E. (1984). The Jan Mayen Ridge: present status. *Polar*  
538 *Research*, 2(1), 47–59. doi:10.1111/j.1751-8369.1984.tb00485.x
- 539 Peron-Pinvidic, G., & Manatschal, G. (2010). From microcontinents to extensional allochthons:  
540 witnesses of how continents rift and break apart? *Petroleum Geoscience*, 16(3), 189–197.  
541 doi:10.1144/1354-079309-903
- 542 Peron-Pinvidic, G., Gernigon, L., Gaina, C., & Ball, P. (2012). Insights from the Jan Mayen  
543 system in the Norwegian-Greenland sea - I. Mapping of a microcontinent. *Geophysical Journal*  
544 *International*, 191(2), 413–435. doi:10.1111/j.1365-246X.2012.05639.x
- 545 Plafker, G., & Berg, H. C. (1994). Overview of the geology and tectonic evolution of Alaska.  
546 *The Geology of Alaska: Geological Society of America*, 989–1021.
- 547 Plummer, P. S., & Belle, E. R. (1995). Mesozoic tectono-stratigraphic evolution of the  
548 Seychelles microcontinent. *Sedimentary Geology*, 96(1–2), 73–91. doi:10.1016/0037-  
549 0738(94)00127-G
- 550 Ricou, L. E. (1994). Tethys reconstructed: plates, continental fragments and their boundaries  
551 since 260 Ma from Central America to South-eastern Asia. *Geodinamica Acta*, 7(4), 169–218.  
552 doi:10.1080/09853111.1994.11105266
- 553 Ritsema, J., van Heijst, H. J., & Woodhouse, J. H. (1999). Complex shear wave velocity  
554 structure imaged beneath Africa and Iceland. *Science*, 286(5446), 1925–1928.  
555 doi:10.1126/science.286.5446.1925
- 556 Roger, J., Platel, J. P., Cavelier, C., & Bourdillon-de-Grisac, C. (1989). Données nouvelles sur la  
557 stratigraphie et l’histoire géologique du Dhofar (Sultanat d’Oman). *Bulletin de La Société*  
558 *Géologique de France*, 2, 265–277. doi:10.2113/gssgfbull.V.2.265
- 559 Schiffer, C., Peace, A., Phethean, J., Gernigon, L., McCaffrey, K., Petersen, K. D., & Foulger, G.  
560 (2018). The Jan Mayen microplate complex and the Wilson cycle. *Geological Society London,*  
561 *Special Publication*, 470, SP470-2. doi:10.1144/SP470.2
- 562 Scrutton, R. A. (1976). Microcontinents and their significance. *Geodynamics: Progress and*  
563 *Prospects*, 5, 177–189.

- 564 Sengör, A. M. C., & Yilmaz, Y. (1981). Tethyan evolution of Turkey: a plate tectonic approach.  
565 *Tectonophysics*, 75(3–4), 181–241. doi:10.1016/0040-1951(81)90275-4
- 566 Sizova, E., Gerya, T., Brown, M., & Perchuk, L. L. (2010). Subduction styles in the  
567 Precambrian: Insight from numerical experiments. *Lithos*, 116(3–4), 209–229.  
568 doi:10.1016/j.lithos.2009.05.028
- 569 Stampfli, G. M., & Borel, G. D. (2002). A plate tectonic model for the Paleozoic and Mesozoic  
570 constrained by dynamic plate boundaries and restored synthetic oceanic isochrons. *Earth and  
571 Planetary Science Letters*, 196(1), 17–33. doi:10.1016/S0012-821X(01)00588-X
- 572 Stampfli, G. M., Von Raumer, J. F., & Borel, G. D. (2002). Paleozoic evolution of pre-Variscan  
573 terranes: From Gondwana to the Variscan collision. *Geological Society of America Special  
574 Paper*, 364, 263–280.
- 575 Takin, M. (1972). Iranian geology and continental drift in the Middle East. *Nature*, 235, 147–  
576 150.
- 577 Torsvik, T. H., Amundsen, H. E. F., Trønnes, R. G., Doubrovine, P. V., Gaina, C., Kuznir, N. J.,  
578 et al. (2015). Continental crust beneath southeast Iceland. *Proceedings of the National Academy  
579 of Sciences*, 112(15), E1818–E1827. doi:10.1073/pnas.1423099112
- 580 Torsvik, T. H., Smethurst, M. A., Burke, K., & Steinberger, B. (2006). Large igneous provinces  
581 generated from the margins of the large low-velocity provinces in the deep mantle. *Geophysical  
582 Journal International*, 167(3), 1447–1460. doi:10.1111/j.1365-246X.2006.03158.x
- 583 Turcotte, D. L., & Schubert, G. (2002). *Geodynamics* (pp. 456). Cambridge, UK: Cambridge  
584 University Press.
- 585 Van Hinsbergen, D. J. J., Langereis, C. G., & Meulen Kamp, J. E. (2005). Revision of the timing,  
586 magnitude and distribution of Neogene rotations in the western Aegean region. *Tectonophysics*,  
587 396(1–2), 1–34. doi:10.1016/j.tecto.2004.10.001
- 588 Van Staal, C. R., Barr, S. M., & Percival, J. A. (2012). Lithospheric architecture and tectonic  
589 evolution of the Canadian Appalachians and associated Atlantic margin. *Tectonic styles in  
590 Canada: the LITHOPROBE perspective. Edited by Percival, J. A., Cook F. A., and Clowes R. M.  
591 Geological Association of Canada, Special Paper*, 49, 41–95.
- 592 Van Staal, C. R., Whalen, J. B., Valverde-Vaquero, P., Zagorevski, A., & Rogers, N. (2009).  
593 Pre-Carboniferous, episodic accretion-related, orogenesis along the Laurentian margin of the  
594 northern Appalachians. *Geological Society, London, Special Publications*, 327(1), 271–316.  
595 doi:10.1144/SP327.13
- 596 Vink, E., Morgen, J. M., & Zhao, W.-L. (1984). Preferential rifting of continents: A source of  
597 displaced terranes. *Journal of Geophysical Research: Solid Earth*, 89(B12), 100072–10076.  
598 doi:10.1029/JB089iB12p10072
- 599 Von Raumer, J. F., Stampfli, G. M. & Bussy F. (2003). Gondwana-derived microcontinents - the  
600 constituents of the Variscan and Alpine collisional orogens. *Tectonophysics*, 365(1–4), 7–22.  
601 doi:10.1016/S0040-1951(03)00015-5.
- 602 Vogt, K., Matenco, L., & Cloetingh, S. (2017). Crustal mechanics control the geometry of  
603 mountain belts. Insights from numerical modelling. *Earth and Planetary Science Letters*, 460,  
604 12–21. doi:10.1016/j.epsl.2016.11.016



- 605 Vogt, K., Willingshofer, E., Matenco, L., Sokoutis, D., Gerya, T., & Cloetingh, S. (2018). The  
606 role of lateral strength contrasts in orogenesis: A 2D numerical study. *Tectonophysics*, 476, 549–  
607 561. doi:10.1016/j.tecto.2017.08.010
- 608 Watchorn, F., Nichols, G. J., & Bosence, D. W. J. (1998). Rift-related sedimentation and  
609 stratigraphy, southern Yemen (Gulf of Aden). In *Sedimentation and Tectonics in Rift Basins Red  
610 Sea:-Gulf of Aden*, 165–189. doi:10.1007/978-94-011-4930-3\_11
- 611 Whittaker, J. M., Williams, S. E., Halpin, J. A., Wild, T. J., Stilwell, J. D., Jourdan, F., &  
612 Daczko, N. R. (2016). Eastern Indian Ocean microcontinent formation driven by plate motion  
613 changes. *Earth and Planetary Science Letters*, 454, 203–212. doi:10.1016/j.epsl.2016.09.019
- 614 Willingshofer, E., Sokoutis, D., Luth, S. W., Beekman, F., & Cloetingh, S. (2013). Subduction  
615 and deformation of the continental lithosphere in response to plate and crust-mantle coupling.  
616 *Geology*, 41(12), 1239–1242. doi:10.1130/G34815.1
- 617 Zhang, N., Zhong, S., Leng, W., & Li, Z. X. (2010). A model for the evolution of the Earth's  
618 mantle structure since the Early Paleozoic. *Journal of Geophysical Research: Solid Earth*, 115,  
619 B6. doi:10.1029/2009JB006896  
620

621 **Figure captions**

622 **Figure 1.** Plate reconstructions and schematic scenarios illustrating two principal types of the  
 623 microcontinents: a) microcontinent formed in a purely extensional tectonic setting: the North  
 624 Atlantic region, separation of the Jan Mayen microcontinent from East Greenland (reconstruction  
 625 after Torsvik et al., 2015); b) microcontinent formed in the context of continuous convergence of  
 626 the plates: Africa and the Neo-Tethys ocean, the Apulian microcontinent detached from Africa  
 627 and then accreted to the Eurasia during ongoing subduction of the Neo-Tethys lithosphere. The  
 628 layer colors on the schematic profiles correspond to the rock types shown on Fig. 2.

629 **Figure 2.** Initial model setup that consists of an overriding continental lithosphere and  
 630 subducting lithospheric plate including both oceanic and continental lithosphere. A mantle plume  
 631 (40-km radius thermal anomaly of 1900-2000°C) is seeded underneath the continental part of  
 632 subducting plate. A weak zone characterized by low plastic strength and wet olivine rheology  
 633 has been implemented in order to provide a rheological decoupling between the upper and  
 634 subducting plate, enabling subduction of the incoming oceanic lithosphere beneath the overriding  
 635 continent (e.g. Burg & Gerya, 2005; Vogt et al., 2017, 2018; Willingshofer et al., 2013). The top  
 636 surface of the lithosphere is defined as an internal free surface through a 12 km-thick layer of  
 637 “sticky air” (Gerya, 2010; Duretz et al., 2011; Cramer et al., 2012). The code “I3ELVIS”  
 638 accounts for mineralogical phase changes by thermodynamic solution for density, obtained from  
 639 the optimization of Gibbs free energy for a typical mineralogical composition of the  
 640 lithospheric/sublithospheric mantle and plume material (Connolly, 2005). Partial melting is  
 641 implemented using the most common parameterization (Katz et al., 2003; Gerya, 2013) of  
 642 hydrous mantle melting processes. The color legend for different types of the rocks includes the  
 643 following: 0 – sticky air, 1 – sediments, 2 – upper continental crust, 3 – lower continental crust, 4  
 644 – oceanic crust/underplated mafic material, 5 – lithospheric mantle, 6 – sublithospheric mantle, 7  
 645 – hydrated continental crust, 8 – hydrated mantle/mantle plume, 9 – melt-bearing continental  
 646 crust, 10 – melt-bearing gabbro, 11 – melt-bearing lithospheric mantle, 12 – melt-bearing  
 647 sublithospheric mantle, 13 – melt-bearing hydrated mantle/mantle plume, 14 – quenched mantle.  
 648 Hydrated, partially molten and quenched rocks not shown on Fig. 2 will appear over the  
 649 evolution of the experiments (see Figs. 3-5).

650 **Figure 3.** Central vertical cross-sections showing the evolution over time for the following  
 651 experiments: a) model 1, no plume; b) model 2, mantle plume of “normal” temperature  
 652 (1900°C); c) model 3, “hot” mantle plume (2000°C); d) model 4, “elevated” continental  
 653 geotherm (1350°C isotherm at 90 km) above “normal” (1900°C) mantle plume. All these  
 654 experiments are characterized by the same velocity of horizontal influx:  $V_x=4.5$  cm/yr. Colors of  
 655 rock types are as on Fig. 2.

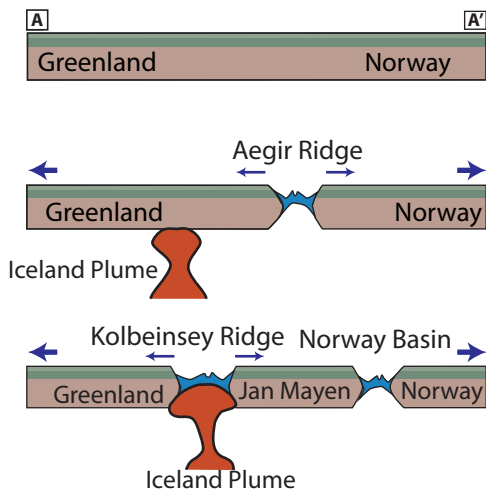
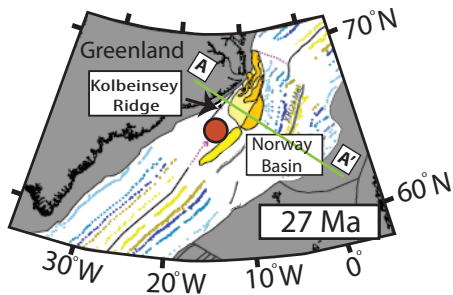
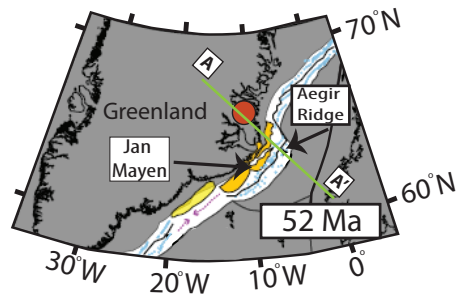
656 **Figure 4.** 3D view of the temporal evolution for the model 4 (“elevated” continental geotherm  
 657 above “normal” mantle plume,  $V_x=4.5$  cm/yr; see Table S1). Colors of rock types are as on Fig.  
 658 2.

659 **Figure 5.** Central vertical cross-sections showing the evolution for the experiments characterized  
 660 by normal temperature of the mantle plume (1900°C), “elevated” continental geotherm (1350°C  
 661 isotherm at 90 km) in the overriding plate and varied velocities of horizontal influx at the right  
 662 model boundary: a) model 5,  $V_x=3.0$  cm/yr; b) model 6,  $V_x=1.5$  cm/yr; c) model 7,  $V_x=0.3$   
 663 cm/yr, d) model 8,  $V_x=0.0$  cm/yr. Note a gradual increase of the maximum width of newly

664 formed oceanic basin from 100 km through 125-175 km to 200 km with decreasing  $V_x$  from 3.0  
665 cm/yr through 1.5-0.3 cm/yr to 0 cm/yr. Colors of rock types are as on Fig. 2.

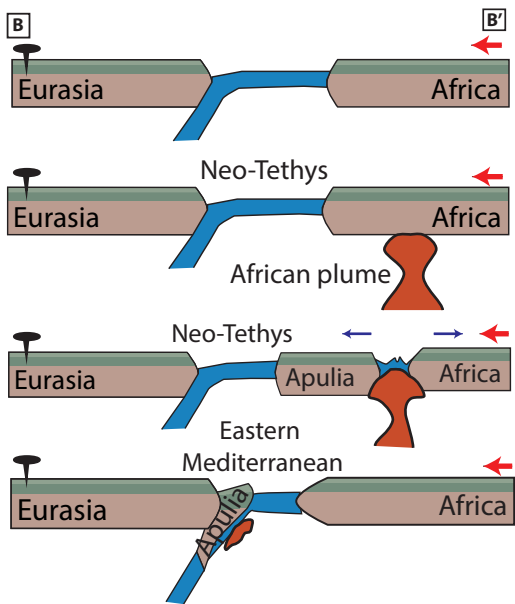
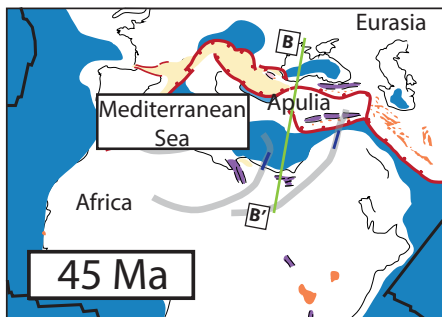
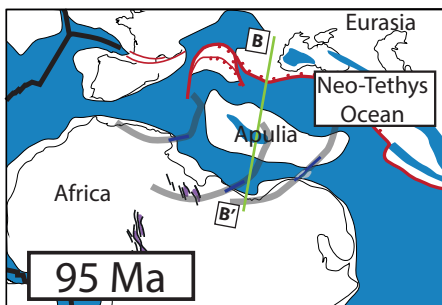
Figure 1.

## a. Divergent tectonic setting



- major continental entity □ oceanic crust
- main tectonic blocks and southward of extension of Jan Mayen microcontinent
- magnetic anomalies ● Iceland plume

## b. Convergent tectonic setting



- major continental entity □ oceanic crust
- active compression
- active rifting
- volcanism
- mid-oceanic ridges
- subduction zone
- motion paths of Africa
- normal faults

Figure 2.

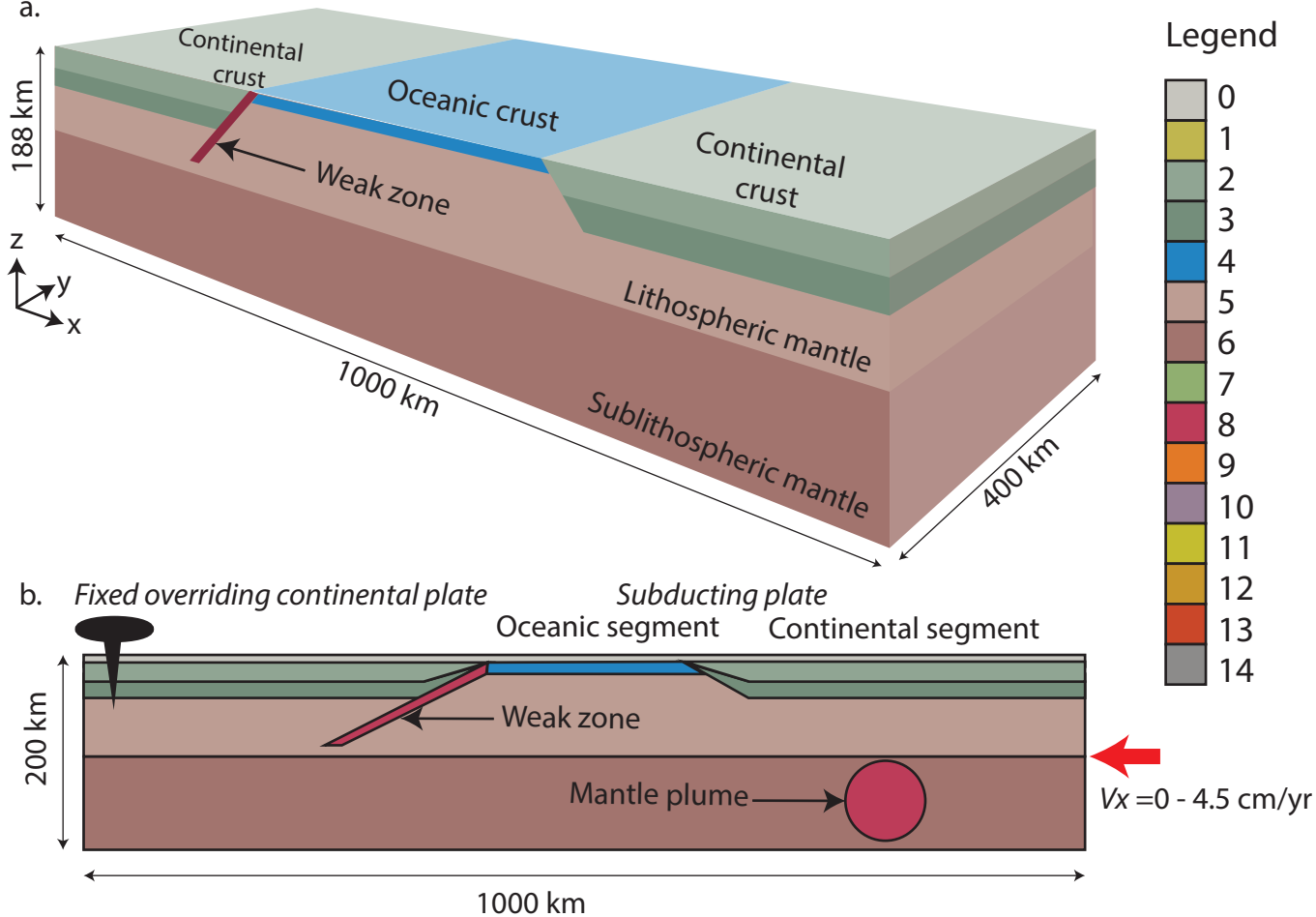
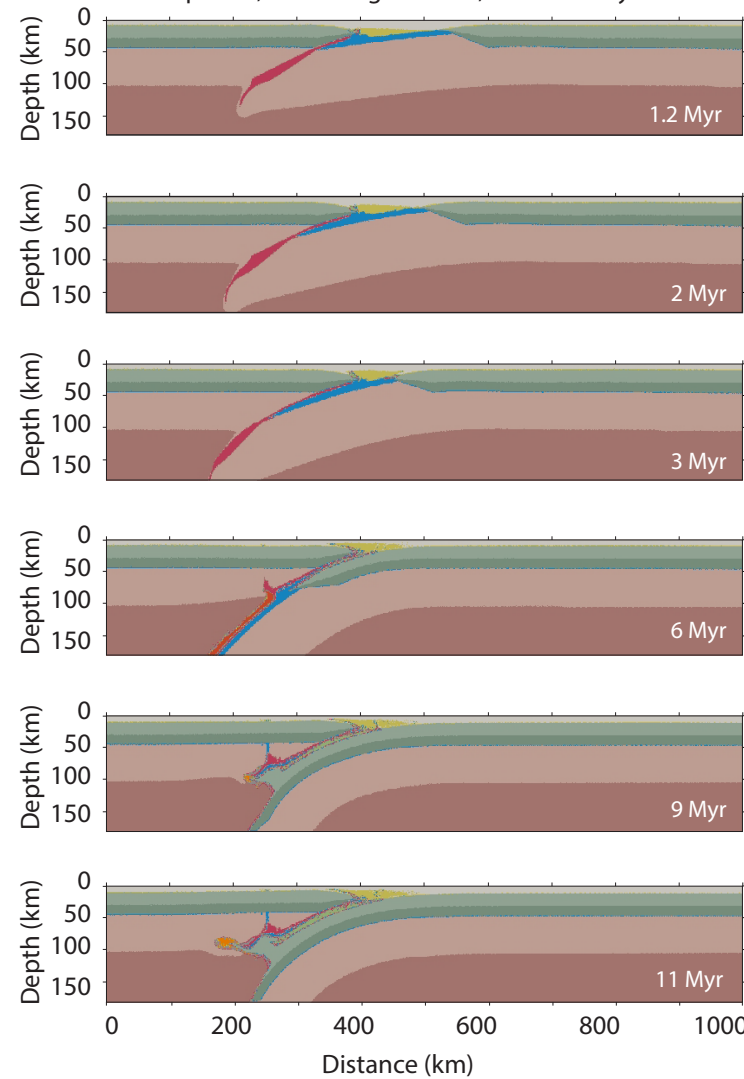


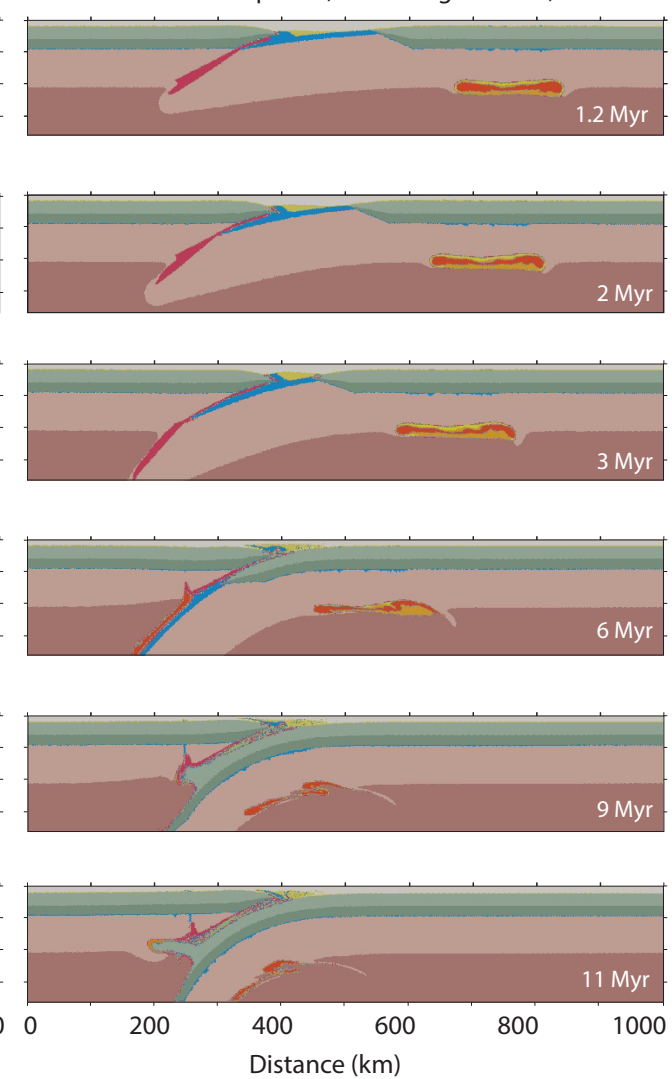
Figure 3.



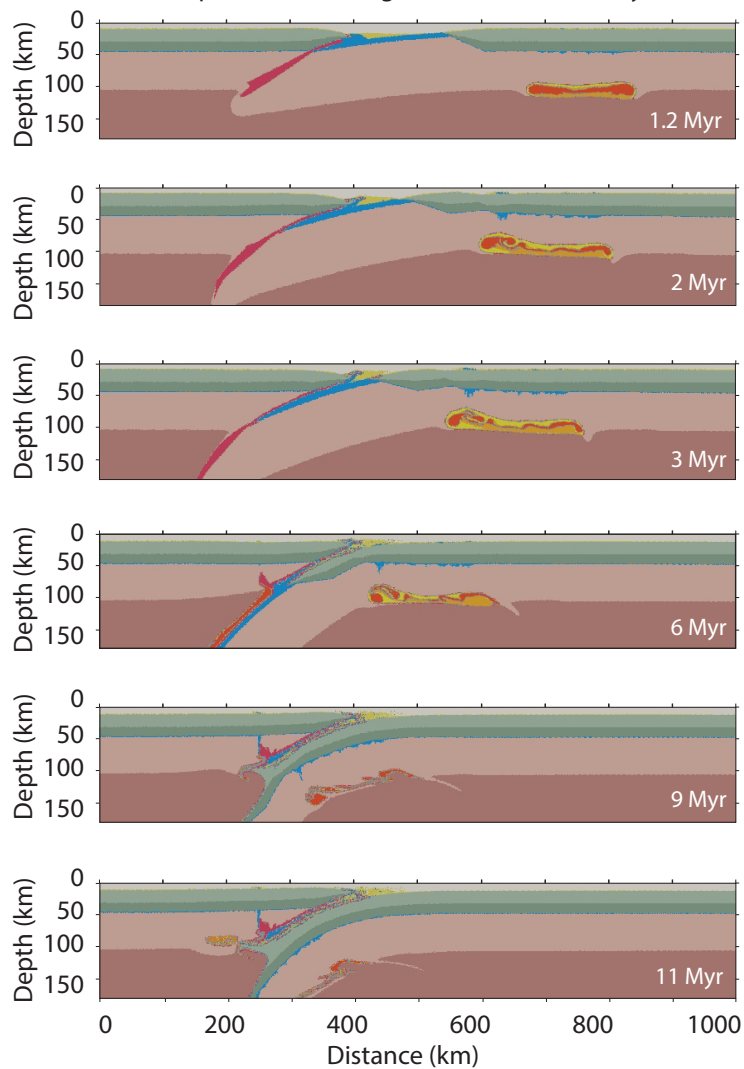
a. **Model 1:** No plume, "normal" geotherm,  $V_x = 4.5$  cm/yr



b. **Model 2:** "Normal" plume, "normal" geotherm,  $V_x = 4.5$  cm/yr



c. **Model 3:** "Hot" plume, "normal" geotherm,  $V_x = 4.5$  cm/yr



d. **Model 4:** "Normal" plume, "elevated" geotherm,  $V_x = 4.5$  cm/yr

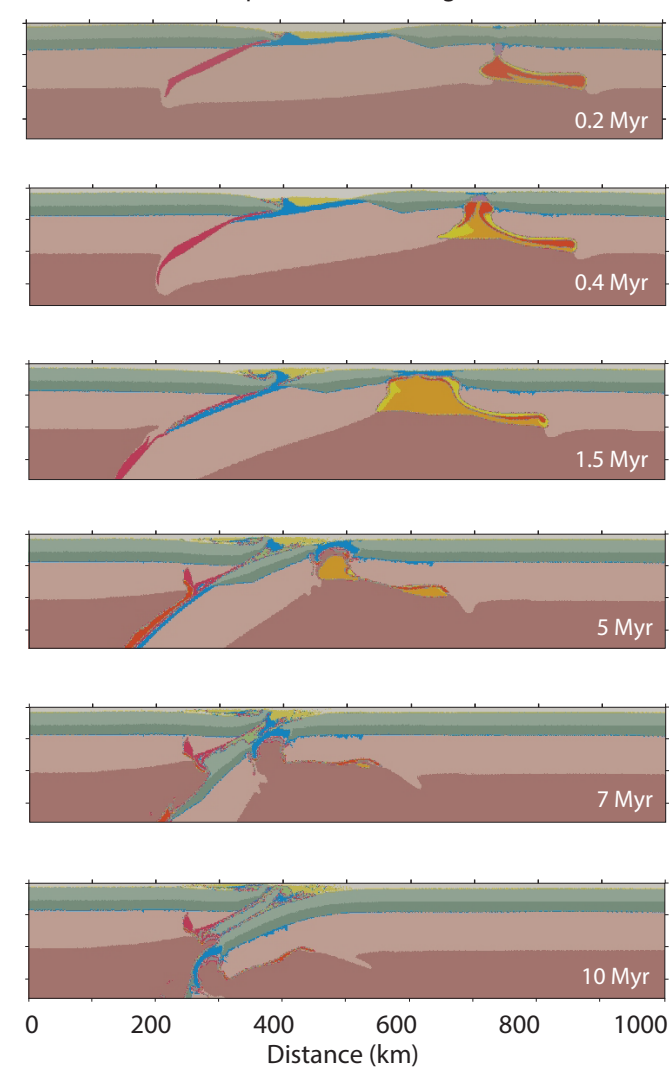
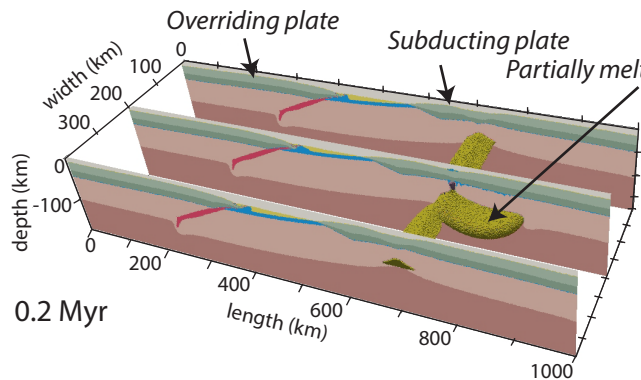
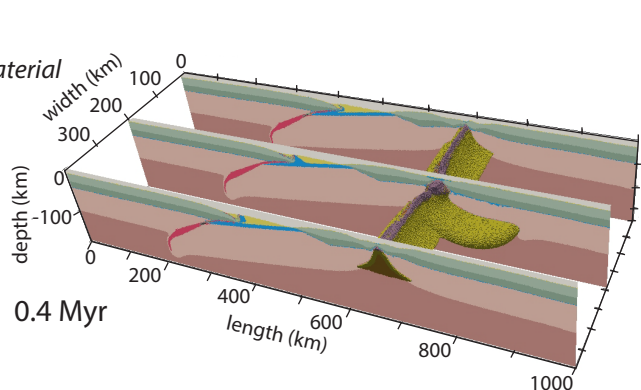


**Figure 4.**

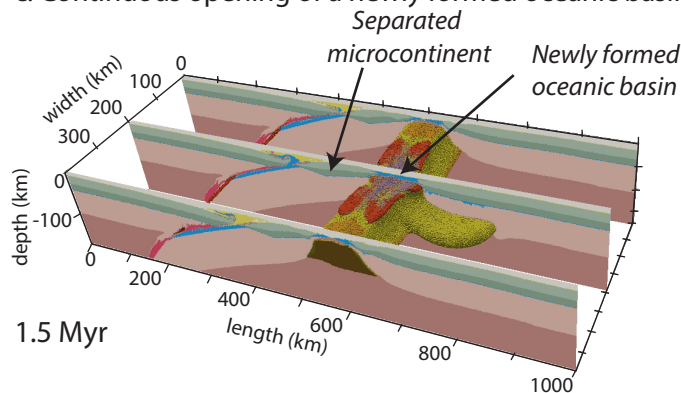
a. Mantle plume uplift leading to decompressional melting of lithospheric and sublithospheric mantle



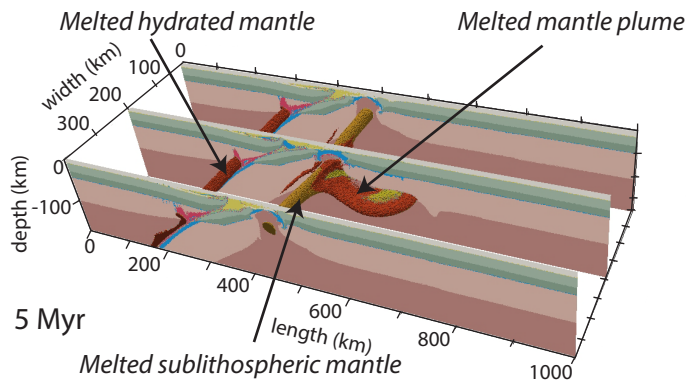
b. Continental break-up and separation of a microcontinent from the main subducting continent



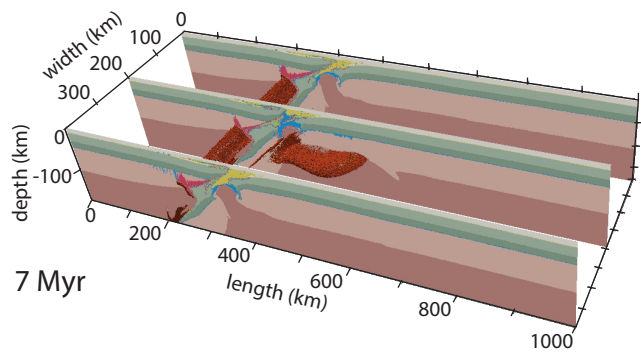
c. Continuous opening of a newly formed oceanic basin



d. Subduction of separated microcontinent



e. Subduction of newly formed basin; start of exhumation of the microcontinental upper crust



f. Exhumation and overthrusting of microcontinental crust onto the subducted crust of the main continent

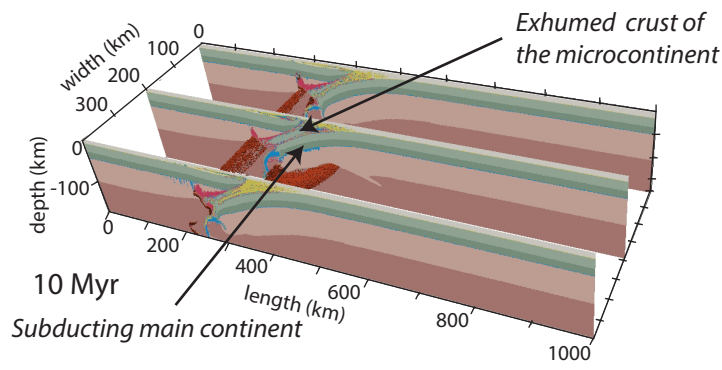
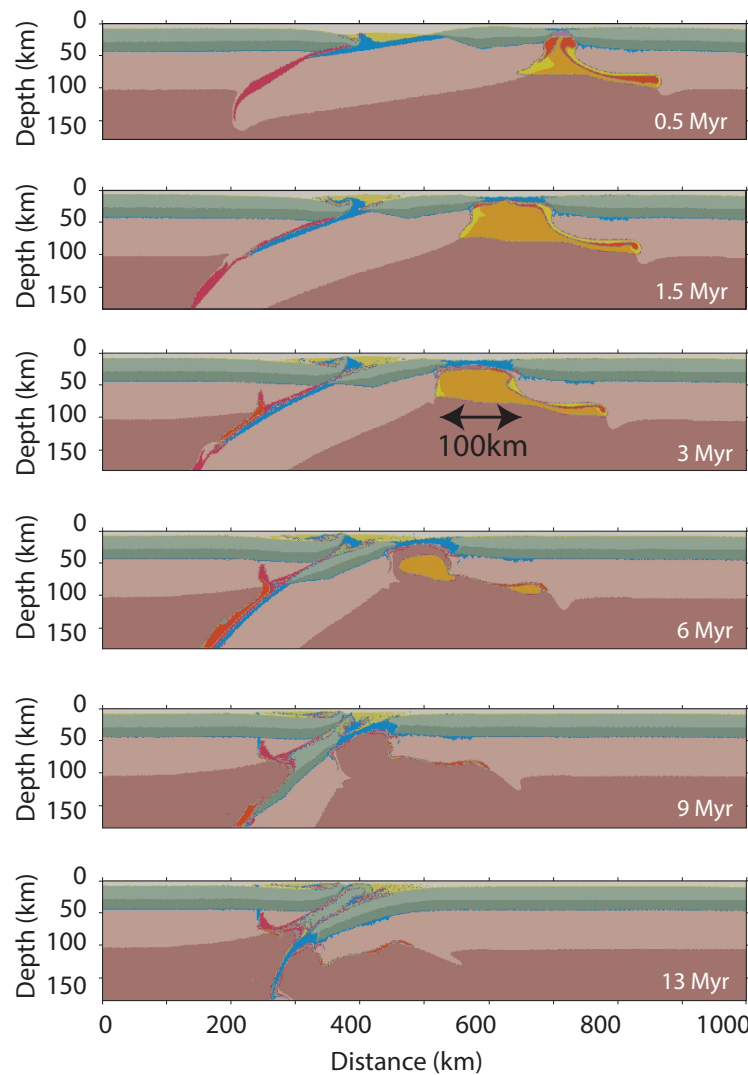
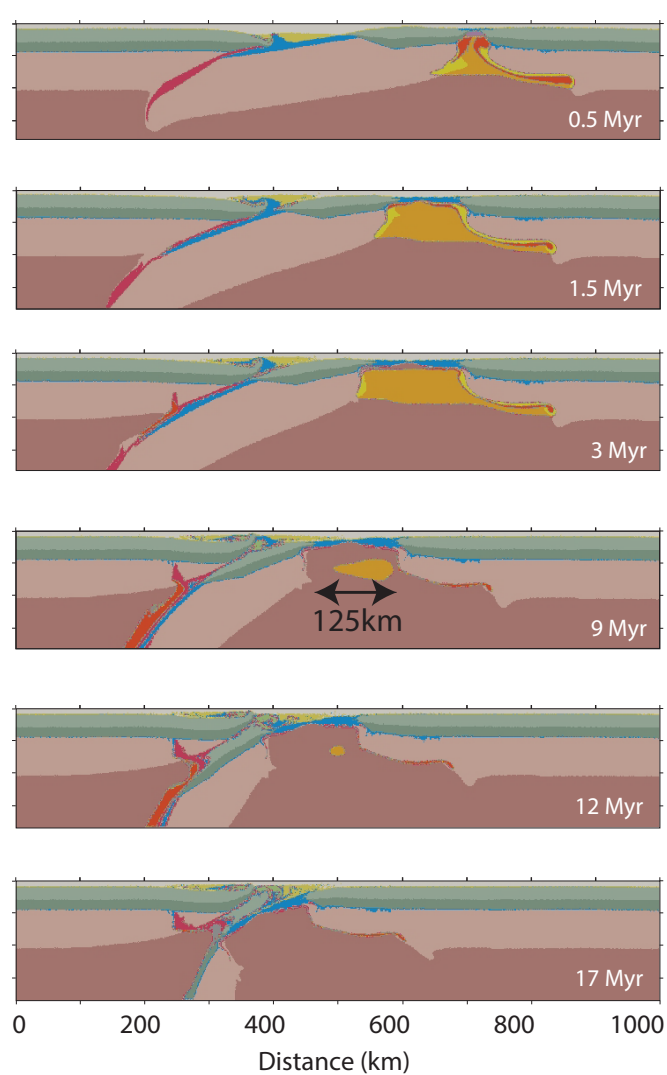
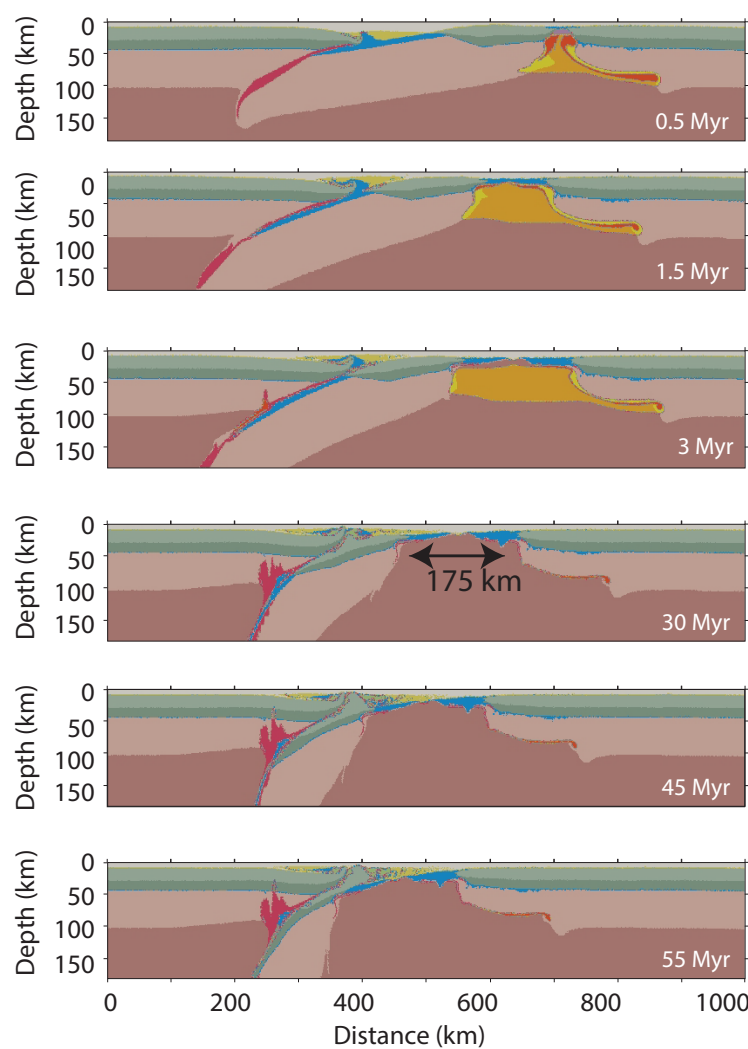


Figure 5.

**a. Model 5** ("Fast" subduction):"Normal" plume, "elevated" geotherm,  $V_x = 3.0$  cm/yr**b. Model 6** ("Intermediate" subduction):"Normal" plume, "elevated" geotherm,  $V_x = 1.5$  cm/yr**c. Model 7** ("Slow" subduction):"Normal" plume, "elevated" geotherm,  $V_x = 0.3$  cm/yr**d. Model 8** ("No push"):"Normal" plume, "elevated" geotherm,  $V_x = 0.0$  cm/yr